Understanding the Influences of Multiscale Waviness on the Elastohydrodynamic Lubrication Performance, Part II: The Partial-Film Condition

Yuechang Wang and Ying Liu *

Posted Date: 25 April 2024

doi: 10.20944/preprints202404.1568.v1

Keywords: thermal elastohydrodynamic lubrication; partial film; multiscale waviness

 doi:10.20944/preprints202404.1568.v1

Article

Understanding the Influences of Multiscale Waviness on the Elastohydrodynamic Lubrication Performance, Part II: The Partial-Film Condition

Yuechang Wang [1] and Ying Liu [2,*]

[1] School of Mechanical Engineering and Automation, Harbin Institute of Technology, Shenzhen 518055, China; wangyuechang@hit.edu.cn
[2] State Key Laboratory of Tribology in Advanced Equipment, Tsinghua University, Beijing 100084, China
* Correspondence: liuying@mail.tsinghua.edu.cn

Abstract: This paper is the second part of a two-part report studying the responses of a typical point-contact elastohydrodynamic lubrication (EHL) problem to multiscale roughness that is mimicked by artificially generated waviness with different amplitudes, frequencies, and directions. The previous Part I paper (doi:10.3390/lubricants10120368) focuses on the full film regime, while the current paper focuses on the partial film regime. The amplitudes and frequencies are related to the feature geometry of smooth EHL problems. Generated waviness is input to a transient thermal EHL model. The simulation is conducted 1,600 times for different waviness parameters, loads, and speeds. Eight performance parameters are extracted: the asperity contact ratio, minimum film thickness, maximum pressure, central point film thickness, central point pressure, mean film thickness, coefficient of friction (COF), and the maximum temperature rise. The ratios of the first seven parameters with and without waviness and the asperity contact ratio values are plotted on the frequency–amplitude coordinate plane as contour maps. The influences of the amplitude, frequency, wave direction, load, and speed on the eight performance parameters are analyzed and summarized. The simulated data and plotted contour maps are provided to the readers in the Supplementary Material.

Keywords: thermal elastohydrodynamic lubrication; partial film; multiscale waviness

1. Introduction

In the previous Part I paper [1], the background and significance of this series of works were thoroughly explained. Regarding the completeness of the current paper, the whole story is briefly repeated here.

In most cases, modeling realistic tribology systems requires surface roughness as a crucial input variable [2]. One fundamental issue of the modeling processes is the realistic representation of the roughness. However, the multiscale nature of roughness, which has drawn the attention of researchers since the work of Archard in 1957 [3], makes it hard to clarify the question: how does one select the appropriate roughness scales relevant to specific tribology systems?

Finding the answers to this question has at least three significant advantages for the tribology community. The first advantage is saving computational resources by modeling tribology systems within the roughness scales that relate to them the most. The second one helps the industry reduce costs and save time by measuring the surface topography of parts on the relevant scales. The third one is improving tribological performance by designing multiscale roughness.

Therefore, the question above has been studied by more and more researchers in recent years. Currently, two kinds of strategies are used to solve the question of how to characterize roughness.

The first category uses the nonstationary random process to describe the multiscale roughness features [4]. Then, in the 1980s, the fractal concepts developed rapidly [5]. As fractal methods show great potential in characterizing the multiscale features by scale-invariant parameters, they were soon used to describe the nonstationary roughness [6]. Then, fractal roughness is successfully used to boost

 doi:10.20944/preprints202404.1568.v1

the studies of the contact mechanics between rough surfaces [7–10]. Researchers found that the roughness scales have disparate effects on different contact quantities. For example, the real contact area and rubber friction dissipation are mainly related to the high-frequency roughness components [11]. Meanwhile, the stiffness and electrical conductance are more relevant to the low-frequency roughness [12,13].

The other category uses the stationary random process to describe roughness. This method started with Longuet-Higgins [14] and Nayak [15]. They build the fundamentals of the modern roughness characterization parameters that are widely used. Compared to nonstationary or fractal roughness characterized by an analytical equation, stationary roughness is characterized by its height probability density (HPD) and power spectral density (PSD). Thus, stationary roughness is much easier to generate numerically. The outcome is a discrete roughness height matrix, which is more popular with modeling lubrication systems. For example, the pioneering work of Patir and Cheng [16–18] and the unified Reynolds equation of Hu and Zhu [19–28] need roughness height matrix data as an essential input variable. However, researchers have seldom discussed the criteria for selecting the scale calculation domain from the perspective of the tribology system. Only a few researchers have noted this problem. Demirci et al. [22] concluded that finer (smaller) scales could result in a smaller friction coefficient of a mixed-point EHL system. Zhang et al. [26] showed that the high cut-off frequency of the fractal roughness significantly influenced the load-carrying capacity.

In summary, few studies have examined the multiscale roughness characteristic of lubricated contact with roughness. Thus, the question of which roughness scales are relevant to a specific lubricated contact problem remains unclear and requires further study.

In order to investigate this question, the authors first selected the point-contact elastohydrodynamic lubrication (EHL) problem as a representative research object. Then, the multiscale roughness is mimicked by a series of single-scale wavy surfaces, such as the classic work of Venner and Lubrecht [29]. These single-scale wavy surfaces are not relevant to any specific multiscale roughness. One can use them as inputs to simulate the EHL system. The corresponding results can be regarded as a reference not limited to a particular multiscale roughness, indicating the comprehensive and standard responses of the EHL system to roughness components of different frequencies and amplitudes.

Therefore, the current study explores the influence of multiscale waviness on the point-contact EHL problem. The results provide a relatively general and comprehensive understanding of the responses of the EHL system to multiscale roughness, which could inspire the further development of new methodologies to identify roughness scales relevant to the studied EHL system. The full film conditions have been reported in the Part I paper [1]. As a continuation of the previous work, this paper focuses on the partial film conditions.

The detailed organization of this article is as follows. First, the theories and methods are briefly introduced. The models and numerical algorithms have been validated in the previous Part I paper [1]. Then, the configuration of the numerical simulations is provided in detail. Finally, the simulation results are analyzed and discussed.

2. Materials and Methods

2.1. Computation Model

The current research uses the same transient thermal EHL model (TEHL) as the previous Part I paper [1], where modeling details can be found. Here, only the critical features of the model are briefly introduced. Viscosity is a function of pressure and temperature that combines the viscosity–pressure (Barus) and viscosity-temperature (Reynolds) relationships. The density–pressure-temperature relationship is considered using the Dowson–Higginson equation. When solving the Reynolds equation, the lubricant is assumed to be Newtonian. When calculating the shear stress and COF, a non-Newtonian behavior is considered based on the shear stress model reported by Bair et al. [30].

Preprints.org (www.preprints.org) | NOT PEER-REVIEWED | Posted: 25 April 2024 doi:10.20944/preprints202404.1568.v1

The solution domain is essential to understanding the waviness parameter settings. Figure 1 shows the solution domain, the same as those used in the previous Part I paper [1]. The coordinate system is defined according to the Hertzian contact zone. The coordinate origin is at the center of the Hertzian contact zone, and the X-direction represents the relative motion direction between the two mating surfaces. The Y-direction is perpendicular to the X-axis. The solution domain is square, with a side length equal to three times the radius of the Hertzian contact zone, b. According to the non-dimensionalization procedures, the non-dimensional solution domain is $X_s \le X \le X_e$ and $Y_s \le Y \le Y_e$, where $X_s = -1.9$, $X_e = 1.1$, $Y_s = -1.5$, and $Y_e = 1.5$. This size of the solution domain has been widely used in the literature to analyze EHL problems [25,31,32]. This solution domain is discretized into $M \times N$ grids, where $M = N = 256$. In particular, M is the number of grids in the X-direction.

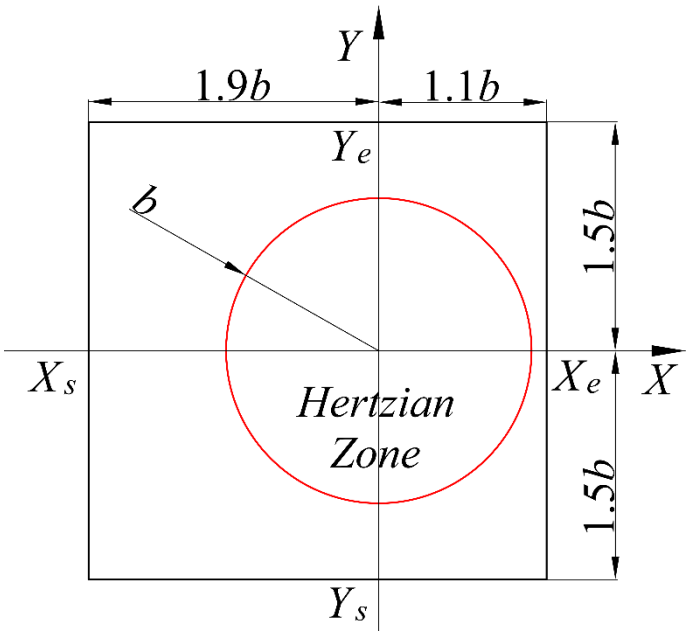

Figure 1. Solution domain of the EHL problem [1].

2.2. Wavy Surface Generation

Three essential parameters are used to generate the wavy surfaces: amplitude, wavelength, and direction. The direction angle θ is the angle between the relative motion direction, X, and the wave direction, X'. Figure 2 shows an illustration of a general wavy surface [1]. When $\theta = 0°$, it represents the transverse waviness. In the case of $\theta = -90°$, longitudinal waviness is generated. The Equation for generating waviness, r_θ, is modified from Venner and Lubrecht, given in Equation (1) [33]:

$$r_\theta(X, Y, \bar{t}) = a_x \cos\left[2\pi \frac{(X - X_d)}{\Lambda_x}\right] \tag{1}$$

$$a_x = \begin{cases} a \times 10^{-10\left[(X - X_d)/\Lambda_x\right]^2}, & \text{if } X - X_d > 0 \\ a, & \text{otherwise} \end{cases} \tag{2}$$

where a is the dimensional amplitude, Λ_x is the non-dimensional wavelength, and the corresponding non-dimensional frequency is $\Omega_x = 2\pi/\Lambda_x$. The amplitude a is modulated to a_x to initiate the waviness with continuous derivatives using Equation (2) [33]. X_d is the location of the start of the waviness. More detailed information about generating waviness can be found in our previous Part I paper [1].

 doi:10.20944/preprints202404.1568.v1

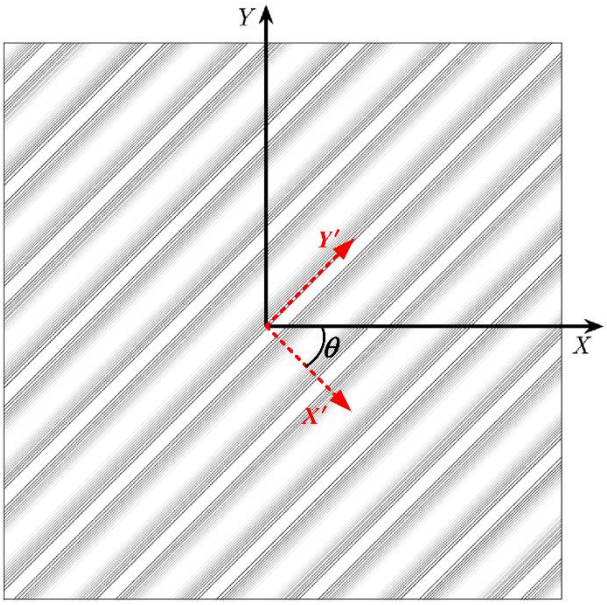

Figure 2. Wavy surface with an arbitrary direction angle [1].

Linking the amplitude and frequency values with the critical features of an EHL problem can provide more meaningful results for identifying the relevant roughness scales. The amplitude, a, is linked with the central film thickness of the smooth EHL problem whose working parameters are the same as those of the EHL problem with wavy surfaces, resulting in the Equation:

$$a = Ah_{cent}^{s} \tag{3}$$

Where A is defined as the non-dimensional amplitude and h_{cent}^{s} represents the central film thickness with the smooth surface.

The wavelength, Λ_x, is linked with the radius of the nominal Hertzian contact zone, b (see Figure 1). In order to further simplify the setting of the wavelength value, the number of waves in the solution domain, N_w, is used to calculate the non-dimensional wavelength, Λ_x, as follows:

$$\Lambda_x = \frac{X_e - X_s}{N_w} \tag{4}$$

Then, the non-dimensional frequency, Ω_x, is calculated as follows:

$$\Omega_x = \frac{2\pi}{\Lambda_x} = \frac{2\pi N_w}{X_e - X_s} = \frac{2\pi N_w}{3} \tag{5}$$

The specific values of A and N_w are provided in Section 2.3. It should be noted that the Ω_x is proportional to the N_w and inversely proportional to the $X_e - X_s$.

2.3. Numerical Simulation Details

The codes used in the current work are verified by the experimental results of He et al. [34]. Detailed verification results can be found in the previous Part I paper [1]. The basic parameters of the EHL simulation are also from the same work listed in Table 1 [1]. The disk and ball are assumed to be made of annealed steel, whose thermal conductivity is 46 W m^{-1}·K^{-1} in Table 1. It should be noted that the hardened steel has a thermal conductivity of approximately 21 W m^{-1}·K^{-1} [35]. Readers should be aware that such a difference in thermal conductivity has been proven to lead to the overestimation of friction under the conditions of a high slide-to-roll ratio (SRR) [36,37]. One should pay attention to the thermal conductivity of the steel if relatively high SRRs are studied.

 doi:10.20944/preprints202404.1568.v1

Table 1. Basic parameters of the EHL simulation [1].

Parameter	Disk (Body 1)	Ball (Body 2)	Fluid
Young's modulus, (GPa)	206	206	
Poisson's ratio	0.3	0.3	
Density, (g/cm3)	7.865	7.865	0.8433
Thermal conductivity, (W/(m·K))	46	46	0.145
Specific heat, (N·m/(g·K))	0.46	0.46	2
Thermal expansivity (K^{-1})			0.00064
Viscosity at 40 °C, (Pa·s)	0.0279		
Temperature–viscosity coefficient, (K^{-1})	0.029		
Pressure–viscosity coefficient, (GPa^{-1})	22.224		
Ball radius, (m)	9.525×10^{-3}		
Slide-to-roll ratio, SRR	−0.2		

The working conditions used in the current work are two load values, w = 200 N and 500 N, and two speeds, u_s = 0.3 m/s and 2 m/s. These parameters result in full film conditions before incorporating the waviness. In the previous Part I paper, the highest speed is u_s = 3 m/s. The current paper reduces the highest speed to 2 m/s due to convergent difficulties dealing with the partial film regimes. The seven key performance parameters of the four working conditions at smooth conditions are listed in Table 2.

Table 2. The seven performance parameters of the four working conditions without waviness.

Load, w (N)	200		500	
Speed, us (m/s)	**0.3**	**2**	**0.3**	**2**
Central film thickness, h_{cent}^{s} (μm)	0.0677	0.2494	0.0628	0.2382
Minimum film thickness, $h_{\min}^{s}$ (μm)	0.0181	0.1029	0.0104	0.078
Average film thickness, h_{mean}^{s} (μm)	0.0617	0.2285	0.0571	0.2165
Central pressure, P_{cent}^{s} (GPa)	1.1128	1.1194	1.5081	1.5141
Maximum pressure, $P_{\max}^{s}$ (GPa)	1.1128	1.1195	1.5081	1.5141
Coefficient of friction, COF^{s}	0.0819	0.0756	0.0882	0.0791
Maximum temperature rise, $t_{\max}^{s}$ (K)	317.97	328.57	321.59	337.44

The amplitude and frequency values used in this work were calculated based on Section 2.2 for each group of load and speed conditions. The non-dimensional amplitude, A, was equal to 2, 2.3, 2.7, 3, 3.3, 3.7, 4, 4.3, 4.7, and 5. The amplitude values are much greater than those used in the Part I paper ($A \in [0.02, 0.3]$) to make the EHL system work in partial film conditions. The frequency values are the same as those in the Part I paper. The N_w values for calculating the frequencies were 2, 6, 9, 12, 16, 19, 22, 25, 29, and 32. The grid convergence study was conducted in the Part I paper [1].

The wave directions used in the current work are the same as those in the Part I paper, which are θ = 0°(transverse), −30°, −60°, and −90°(longitudinal). Each group of amplitude and frequency conditions was used to simulate wavy surfaces with these four different wave directions, representing the rotation of the waviness from transverse to longitudinal.

The time interval of the simulation, $\Delta\bar{t}$, is set to the value that is equal to the shifting of the wavy surface by the distance of one grid, calculated as follows:

$$\Delta\bar{t} = \frac{u_s\left(X_e - X_s\right)}{2u_2\left(M-1\right)} \tag{6}$$

 doi:10.20944/preprints202404.1568.v1

This means that at each time step, the entire wavy surface moves the distance of one grid in the X-direction. The time step for the termination of the simulation, N_T, is set as $N_T = 3 \times M = 768$ to obtain a stable solution to the transient EHL problem. In the previous Part I, the results show that this N_T value is sufficient to obtain a stable solution to the transient EHL problem. The simulations were run at the Center of High-Performance Computing Clusters at Tsinghua University. The CPU time varies from a dozen to 100 h for different combinations of the waviness parameters, load, and speeds. We took advantage of the clusters by running several programs with varying parameter combinations simultaneously.

Based on the transient simulation results, eight critical performance parameters were extracted to characterize the responses. The first seven are the same as those in the previous Part I paper: minimum film thickness, maximum pressure, central film thickness, mean film thickness, maximum temperature rise, and coefficient of friction (COF). The eighth parameter is the asperity contact ratio when the system works in the partial film regime.

3. Results and Discussion

The ratios of the first seven parameters with and without waviness and the asperity contact ratio values were calculated and plotted as contour maps on the frequency–amplitude ($\Omega_x - A_x$) coordinate plane as contour maps with the double logarithm scale to highlight the influence of wavy surfaces on the EHL performance. In order to ensure the brevity and clarity of this article, only representative plots are shown in this section. All the plots and the simulation data used to plot them are included in Supplementary Material S1.

3.1. The Influences of the Waviness Amplitude and Frequency

This section discusses the results simulated with $w = 200$ N, $u_s = 2$ m/s, and $\theta = 0°$ in detail as an example to show the waviness amplitude and frequency effects, primarily when the systems work in the mixed lubrication regime. Figures 3 and 4 show the eight contour maps and Table 3 lists the corresponding range of values shown in the contour maps, rounded to three decimal places.

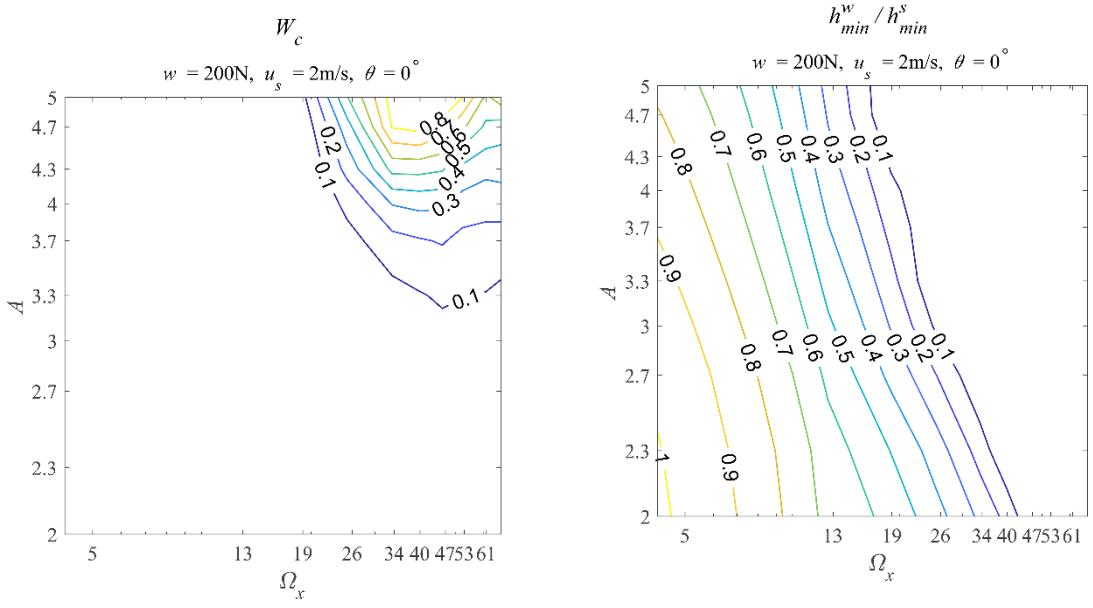

(**a**) (**b**)

 doi:10.20944/preprints202404.1568.v1

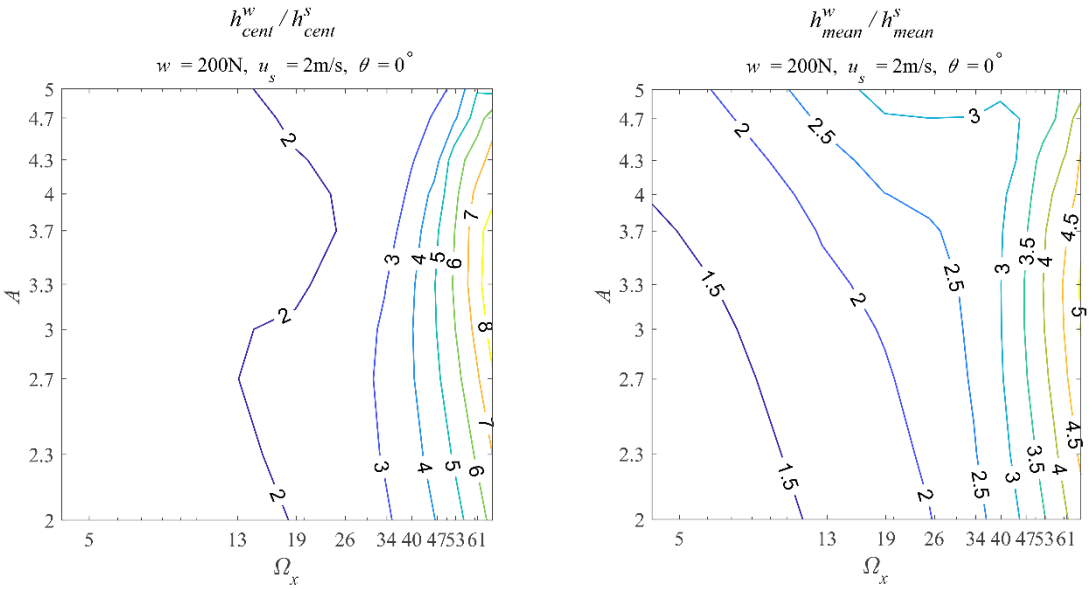

(**c**) (**d**)

Figure 3. Contour maps of asperity contact ratio and those related to the film thickness parameters, w = 200 N, u_s = 2 m/s, θ = 0°, (**a**) W_c, (**b**) $h^w_{\min}/h^s_{\min}$, (**c**) h^w_{cent}/h^s_{cent}, and (**d**) h^w_{mean}/h^s_{mean}.

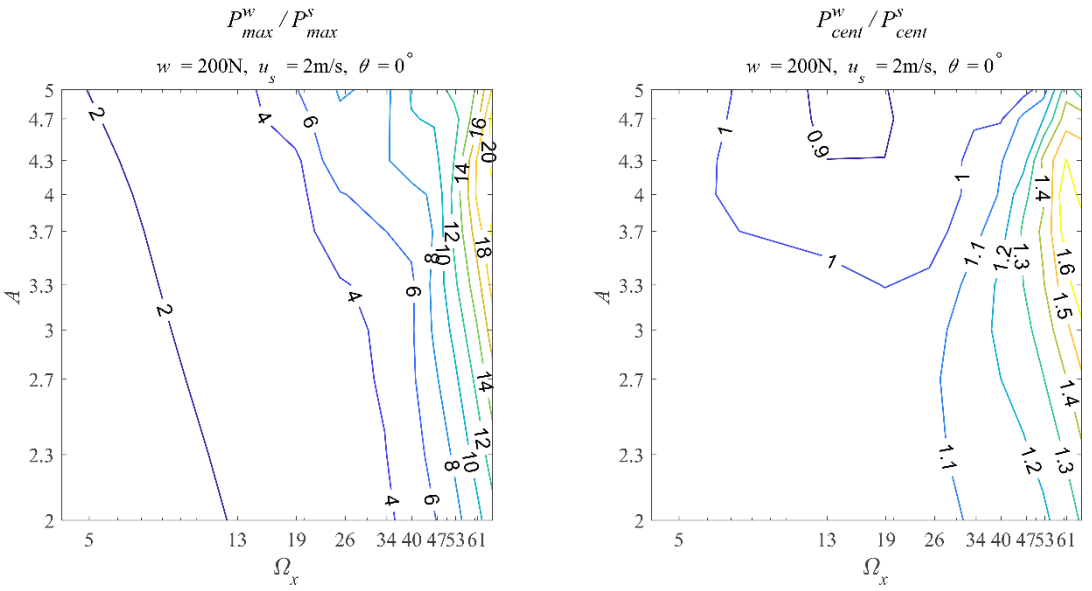

(**a**) (**b**)

Preprints.org (www.preprints.org) | NOT PEER-REVIEWED | Posted: 25 April 2024 doi:10.20944/preprints202404.1568.v1

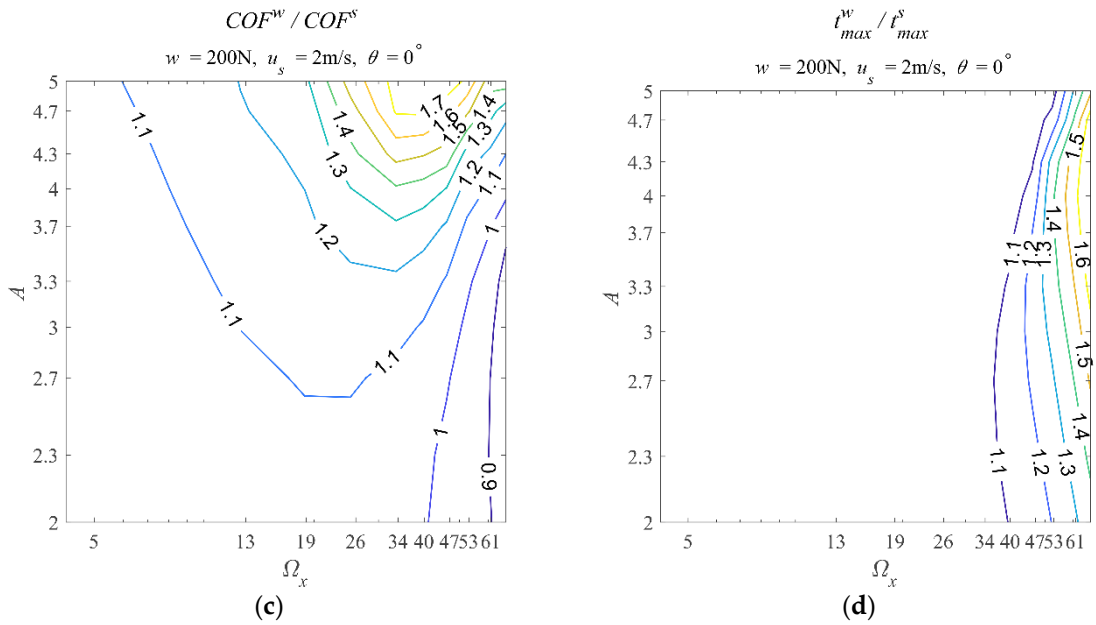

Figure 4. Contour maps of the pressure parameters, friction coefficient, and the maximum temperature rise, $w = 200$ N, $u_s = 2$ m/s, $\theta = 0°$, (**a**) $P^w_{\max}/P^s_{\max}$, (**b**) P^w_{cent}/P^s_{cent}, (**c**) COF^w/COF^s, and (**d**) $t^w_{\max}/t^s_{\max}$.

Table 3. The range of performance parameter ratios obtained with $w = 200$ N, $u_s = 2$ m/s, and $\theta = 0°$.

Parameter	Min	Max
Minimum film thickness ratio, $h^w_{\min}/h^s_{\min}$	0	1.016
Central film thickness ratio, h^w_{cent}/h^s_{cent}	1.150	8.799
Average film thickness ratio, h^w_{mean}/h^s_{mean}	1.132	5.056
Maximum pressure ratio, $P^w_{\max}/P^s_{\max}$	1.242	20.808
Central pressure ratio, P^w_{cent}/P^s_{cent}	0.875	1.699
COF ratio, COF^w/COF^s	0.847	1.766
Maximum temperature rise ratio, $t^w_{\max}/t^s_{\max}$	1.007	1.680
Asperity contact ratio, W_c	0	0.900

The contour maps of the asperity contact ratio and those related to the film thickness parameters are shown in Figure 3. In Figure 3a, the asperity contact ratio shows that the system runs into the partial film regime as the amplitude and frequency increase. The maximum asperity ratio is around 0.9 (Table 3), meaning severe asperity contacts. It should be noted that many full film cases are still shown in Figure 3a, such as ($\Omega_x \approx 13$, $A = 3.3$) and ($\Omega_x \approx 19$, $A = 3$). Such results are unexpected because the waviness amplitude has been three times the central film thickness of the corresponding smooth EHL situations. So, the simulation results shown here illustrate the power of the micro-EHL effects at the asperity scale.

Moreover, the maximum asperity ratio occurs at $\Omega_x \approx 46$ and A = 5. The corresponding amplitude value is the maximum amplitude used in this work. However, the corresponding frequency value is among the frequency range used. This phenomenon means the asperity contact ratio increases as the frequency rises to a maximum value. Then, as the frequency further increases, the asperity contact ratio decreases. Also, this result illustrates that even in the partial film regime where asperity contacts occur, high-frequency waviness can enhance the micro-EHL effects.

Figure 3b shows that the $h^w_{\min}/h^s_{\min}$ values are less than one in most cases, meaning the minimal film thickness is reduced when waviness is incorporated. The result is the same as the full film

 doi:10.20944/preprints202404.1568.v1

condition discussed in the Part I paper [1]. However, the maximum h^w_{min}/h^s_{min} value seems greater than one (1.016 in Table 3), meaning the minimum film thickness is enhanced when considering the designated waviness with relatively small amplitude and frequency ($\Omega_x \approx 4.2$ and $A = 2$). Such results were not in our previous studies within the full film regime. The frequency range is the same for the full (Part I paper) and partial film simulations (current work). The enhancement of minimal film thickness should be due to the amplitudes used. The amplitudes used in the current work are between $A = 2$ and $A = 5$. The amplitude range used in our previous work is between 0.02 and 0.3. Therefore, it can be inferred that when the amplitude value is significant to a certain extent, and the frequency is minor, the waviness can slightly increase the minimum film thickness.

Another point is that the minimal film thickness decreases monotonically till zero (Table 3) as the amplitude and frequency increase. This phenomenon is different from the results shown in our previous work (Part I paper). In Part I, the minimal film thickness first decreases and then increases as the frequency increases. Such a difference means the minimal film thickness won't be enhanced by increasing frequency when the system works in the partial film regime.

Figure 3c shows that the h^w_{cent}/h^s_{cent} ratio values are more significant than one, indicating that the central film thickness is enhanced when waviness is incorporated. Generally, the h^w_{cent}/h^s_{cent} ratio increases as A or Ω_x increases. Within the simulated ranges of A and Ω_x, the maximum h^w_{cent}/h^s_{cent} value is around 8.799 (Table 3), corresponding to $\Omega_x \approx 67$ and $A = 3.3$. The frequency value has reached the upper-frequency limit used in this work. The amplitude value is at the middle of the amplitude range. This result means that an amplitude value exists that enhances the central film thickness the most. In other words, the central film thickness is more sensitive to waviness amplitude.

The contour map of the mean film thickness ratio (Figure 3d) has a similar pattern to that of the central film thickness (Figure 3c). The h^w_{mean}/h^s_{mean} ratio values are greater than one, meaning the waviness can enhance the mean film thickness. In general, the h^w_{mean}/h^s_{mean} ratio increases as A or Ω_x increases. Within the simulated ranges of A and Ω_x, the maximum h^w_{mean}/h^s_{mean} value is around 5.056 (Table 3), corresponding to $\Omega_x \approx 67$ and $A = 3.3$. This pair of amplitude and frequency is the same as that corresponds to the maximum h^w_{cent}/h^s_{cent} value. It is expected that the maximum h^w_{mean}/h^s_{mean} value (5.056) is smaller than the maximum h^w_{cent}/h^s_{cent} value (8.799). Moreover, a specific amplitude value still enhances the mean film thickness the most, just like the situation in the central film thickness. Thus, the mean film thickness can be considered more sensitive to waviness amplitude.

When comparing the contour maps of the central and mean film thicknesses between the partial (this paper) and full (Part I paper) film conditions, the most significant difference is the amplitude and frequency values corresponding to their maxima. In our previous work, where the amplitude range is between 0.02 and 0.3, the amplitude and frequency corresponding to the maximum central and mean film thickness ratios are at the right-up corner of the contour map, representing the maximum frequency and amplitude used in the simulations. However, in this work ($A \in [2,5]$), the maximum h^w_{cent}/h^s_{cent} and h^w_{mean}/h^s_{mean} values are obtained with the maximum frequency and a medium amplitude ($A = 3.3$). Such a difference illustrates that as the amplitude continuously increases, the central and mean film thickness won't monotonically increase. The central and mean film thickness will decrease when the asperity contact ratio is high enough. As for the frequency value, it is clear that within the frequency range used, the higher the frequency is, the greater the enhancement of central and mean film thickness.

In summary, when the point contact EHL system runs into the partial film regime, the waviness can increase the central and mean film thickness but decrease the minimum film thickness in most cases. The central film thickness is the film thickness at the fixed central point ($X = 0, Y = 0$) in the solution domain. The mean film thickness is the average value of the film thickness values within the nominal Hertzian contact zone. The increase in the central and mean film thickness proves that incorporating waviness can further lift the ball, enhancing the EHL effect. As the name suggests, the minimum film thickness is the minimum value of the film thickness distribution. The decreased

 doi:10.20944/preprints202404.1568.v1

minimum film thickness indicates that the lifting effect of the ball is inadequate to counteract the effects of the wave valleys on the minimum film thickness. The decrease in the minimum film thickness is usually considered to be a degradation of the EHL performance.

It should be highlighted that the minimal film thickness can be enhanced with the minimum frequencies and amplitude ($\Omega_x \approx 4.2$ and $A = 2$) used in the simulations with $w = 200$ N, $u_s = 2$ m/s, and $\theta = 0°$. Therefore, one can have a specific situation in which the central, mean, and minimum film thickness all increase by controlling the amplitude and frequency of the waviness. That is the waviness with $\Omega_x \approx 4.2$ and $A = 2$. In our previous paper [1], the recommended waviness parameters were the maximum frequency ($\Omega_x \approx 67$) and maximum amplitude ($A = 0.3$) used in the simulations for the EHL problem with $w = 200$ N, $u_s = 3$ m/s, and $\theta = 0°$. Such an opposite recommendation is due to the lubrication regime and the amplitude range considered. Therefore, one should remember that when approaching the partial film regime by increasing the waviness amplitudes, the best choice of amplitudes and frequencies to enhance the EHL effects needs to be re-examined.

Figure 4 shows the contour maps of ratios of the pressure parameters, friction coefficient, and the maximum temperature rise with and without waviness. Figure 4a shows that the $P^w_{\max}/P^s_{\max}$ ratios are greater than one, indicating that incorporating waviness results in a more significant maximum pressure. When the A or Ω_x increases, the $P^w_{\max}/P^s_{\max}$ ratio increases. The maximum $P^w_{\max}/P^s_{\max}$ value is approximately 20.808, again occurring at the point with the maximum frequency ($\Omega_x \approx 67$) and an intermediate amplitude value ($A = 4.7$), nearing the maximum amplitude used in the simulations. Such results suggest that increasing the amplitude or frequency results in a higher maximum pressure in most cases. Increasing them has synergistic effects in enhancing the maximum pressure. Moreover, the maximum $P^w_{\max}/P^s_{\max}$ value here exceeds our previous Part I paper. The reason should be that the amplitudes used here are much greater than those in the Part I paper.

If one looks at Figures 4a and 3a simultaneously, it can be found that the maximum pressure occurs when the asperity contact occurs. However, the maximum pressure and maximum asperity contact ratios have different corresponding frequencies and amplitudes. The maximum asperity ratio occurs at $\Omega_x \approx 46$ and A = 5, while the maximum $P^w_{\max}/P^s_{\max}$ value occurs at $\Omega_x \approx 67$ and A = 4.7. Generally, researchers prefer to think the larger the asperity contact ratio is, the higher the maximum contact pressure will be. Thus, such a difference challenges this common idea and suggests one should consider the asperity contact ratio and maximum pressure separately.

Furthermore, Figure 3 has shown that waviness with a high frequency and large amplitude can generate a thicker lubricant film in terms of the central and mean film thickness. At the same time, Figure 4a shows that such cases lead to more significant maximum pressure. Maximum pressure increases are usually regarded as unfavorable in an EHL system. Thus, it is necessary to comprehensively consider the influences of waviness on the film thickness and pressure when one wishes to utilize waviness to enhance the EHL effects.

Figure 4b shows the central point pressure ratios (P^w_{cent}/P^s_{cent}) with and without waviness. The P^w_{cent}/P^s_{cent} results fluctuate between 0.875 and 1.699. This range is around one and much smaller than that of the $P^w_{\max}/P^s_{\max}$ (between 1.242 and 20.808). Moreover, the fluctuation of the P^w_{cent}/P^s_{cent} ratios is more relevant to the change in the frequencies. Such results are similar to that in the Part I paper. The central pressure is the pressure at the fixed central point. Its value is more dominated by the maximum Hertzian contact pressure, a constant in a given EHL problem. Therefore, whether in the full or partial film regime, the P^w_{cent}/P^s_{cent} ratio contour map provides less information than the $P^w_{\max}/P^s_{\max}$ ratio contour map.

Figure 4c shows the ratios of the COF with and without waviness (COF^w/COF^s). The COF^w/COF^s ratios vary from 0.847 to 1.766. It is clear that the COF ratio increases first and then decreases as the frequency increases. As for the amplitude, increasing it increases the COF ratio within the simulations of the current work. Thus, the minimum COF ratio occurs at $\Omega_x \approx 67$ and $A = 2.7$, a waviness with a high frequency and small amplitude. The maximum COF ratio occurs at $\Omega_x \approx$

 doi:10.20944/preprints202404.1568.v1

40 and $A = 5$. This specific combination of frequency and amplitude is close to the parameters leading to the maximum asperity contact ratio (Figure 3a, $\Omega_x \approx 46$ and $A = 5$). This phenomenon indicates that the maximum COF mainly depends on the asperity contact ratio when the system works in the partial film regime.

It should be highlighted that in our Part I paper, where the amplitude is relatively small ($A \in [0.02, 0.3]$), the COF^w/COF^s decreases to smaller than one as the amplitude and frequency increase. Such a vast difference should be due to the differences in the composition of friction force between full and partial film regimes. The friction force in the full film regime is merely the viscous shear force within lubricants. In the partial film regime, the friction force comprises the lubricant's viscous shear and the solid friction between asperities. The solid friction between asperities is much greater than the viscous shear force. Therefore, once the asperity contacts are severe to a certain extent, the solid friction between them will dominate the comprehensive friction. Furthermore, it can be concluded that once the EHL system runs in the partial film regime, it would be better to have a relatively smooth surface topography to reduce the COF.

Figure 4d shows that the $t^w_{\max}/t^s_{\max}$ ratios are greater than one, indicating that incorporating waviness results in a higher temperature rise in the lubricated zone. The $t^w_{\max}/t^s_{\max}$ ratio seems to be more sensitive to the frequency values. As the frequency increases, the $t^w_{\max}/t^s_{\max}$ ratio increases significantly. When increasing the amplitude, the $t^w_{\max}/t^s_{\max}$ ratio slightly increases and then decreases. It is worth reminding readers that the results in the Part I paper show that the increasing of $t^w_{\max}/t^s_{\max}$ value leads to decreasing viscosity, then reducing the COF when the EHL system is within the full film regime. This relationship is still valid in the current work, although the asperity contacts occur. The maximum $t^w_{\max}/t^s_{\max}$ ratio is approximately 1.680 when $\Omega_x \approx 67$ and $A = 3.7$. The COF and asperity contact ratios corresponding to this specific frequency and amplitude are around 0.921 and 0.144, respectively. This result means that even when the asperity contacts occur, one can still obtain a reduction of COF by designing the amplitude and frequency of waviness to decrease the viscosity by increasing the temperature.

Combining the information in Figures 3 and 4, when the amplitude increases to initiate asperity contacts, generally, waviness with a high frequency and large amplitude can generate severe asperity contact ratio, a thicker lubricant film in terms of the mean and central film thickness, with a higher maximum pressure, and result in a greater COF, with a higher temperature rise. Generally, a thick lubricant film and small COF are positive results, but high maximum pressure and temperature rise are negative when studying EHL problems. Incorporating waviness can affect them simultaneously. Thus, the conclusion as to whether waviness benefits or does not benefit an EHL problem cannot be drawn directly. After comprehensively considering these pros and cons, one may decide whether incorporating waviness will benefit their studies.

3.2. The Influence of the Wave Direction

The results simulated with $w = 200$ N and $u_s = 2$ m/s are used to discuss the influence of the wave direction. In order to highlight the influences of the wave directions, two cross lines of each contour map were extracted, which are the lines with fixed $A = 3.7$ or fixed $N_w = 19$ ($\Omega_x \approx 39.8$). Then, the extracted lines with the same performance parameters were plotted in one graph. In each graph, the four curves correspond to the four directions $\theta = 0°$, $-30°$, $-60°$, and $-90°$. There are sixteen such graphs organized as sub-figures in Figure 5. Indices a to h represent the eight performance parameters, where '1' and '2' indicate the results of the fixed $N_w = 19$ and $A = 0.09$, respectively.

 doi:10.20944/preprints202404.1568.v1

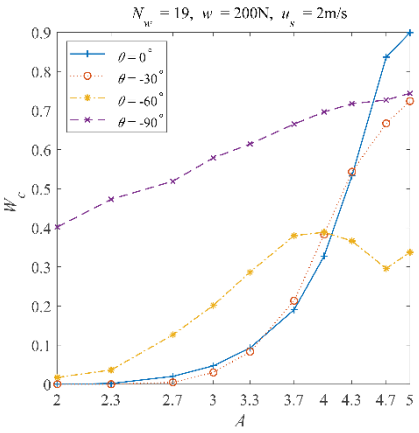

(a.1)

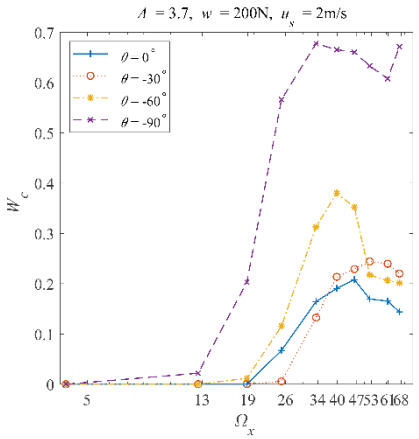

(a.2)

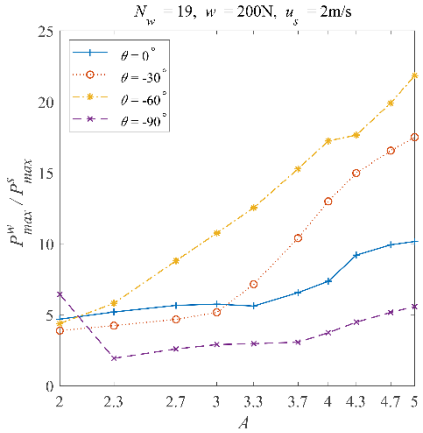

(e.1)

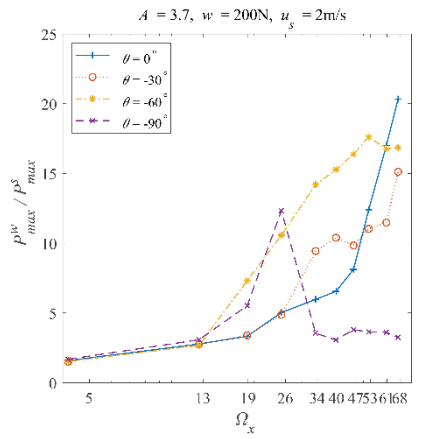

(e.2)

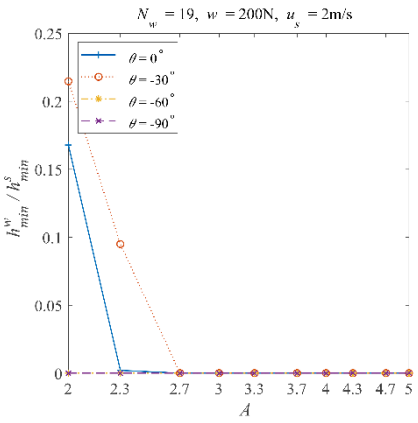

(b.1)

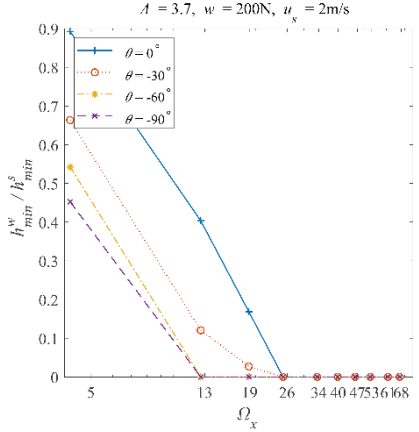

(b.2)

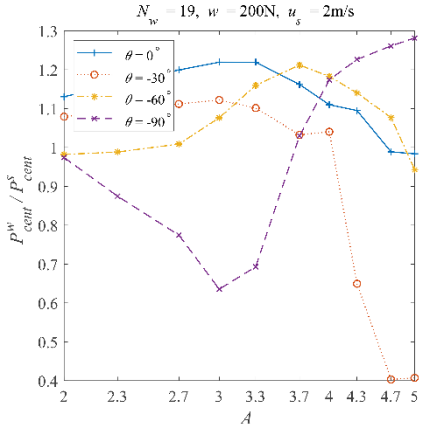

(f.1)

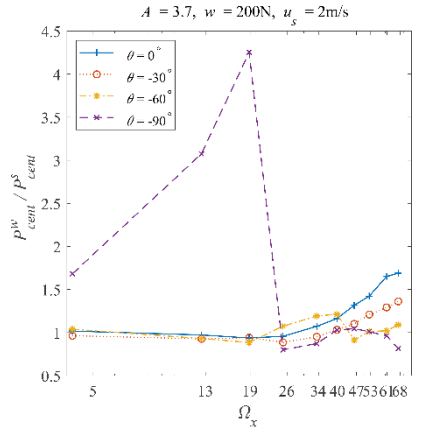

(f.2)

 doi:10.20944/preprints202404.1568.v1

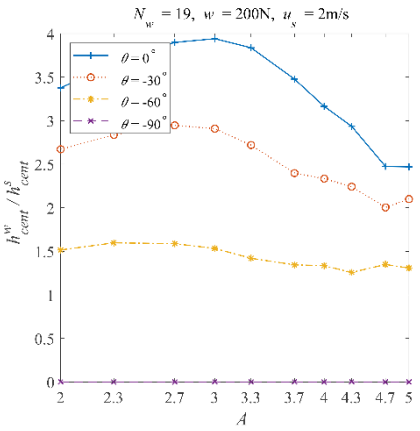

(c.1)

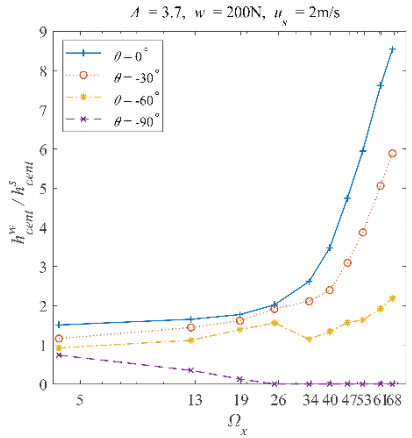

(c.2)

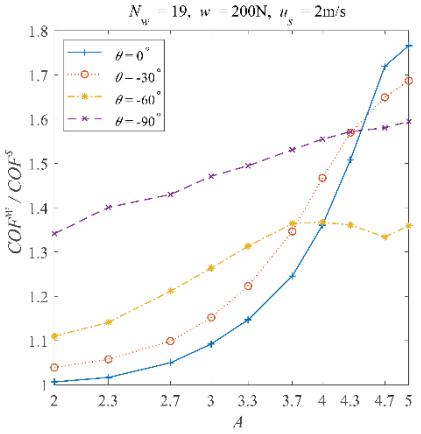

(g.1)

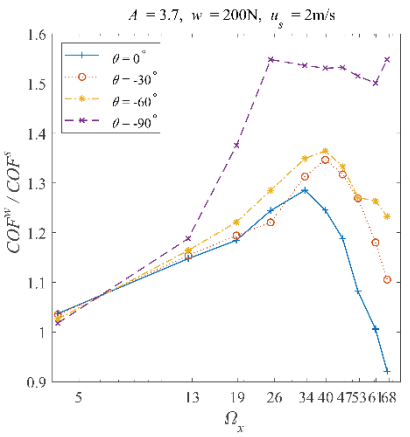

(g.2)

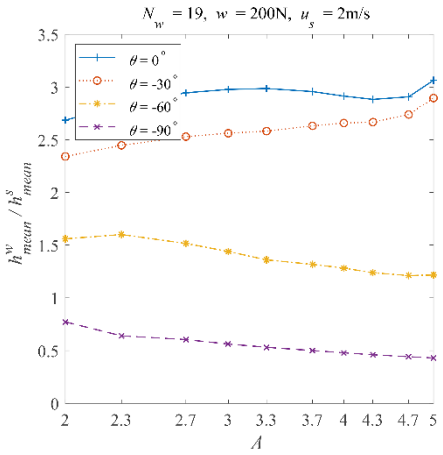

(d.1)

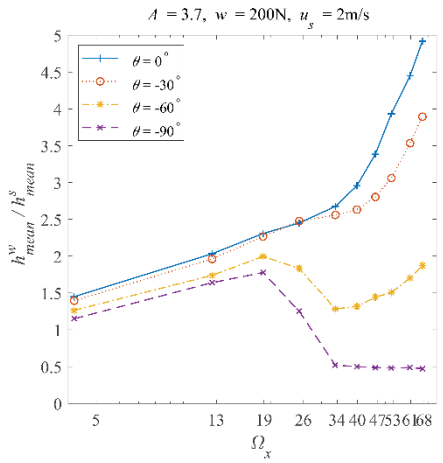

(d.2)

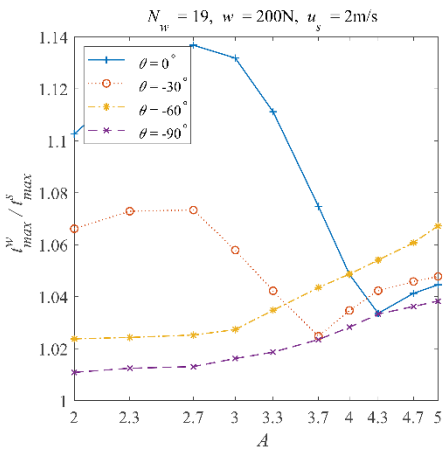

(h.1)

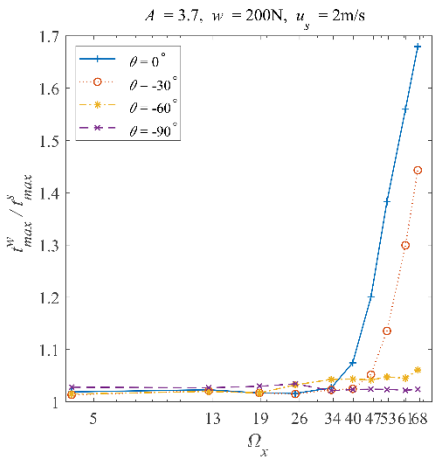

(h.2)

Figure 5. Performance parameters with w = 200 N, u_s = 2 m/s, θ = 0°, −30°, −60°, and −90°. Here, a to h are (**a**) W_c , (**b**) $h^w_{\min}/h^s_{\min}$, (**c**) h^w_{cent}/h^s_{cent} , (**d**) h^w_{mean}/h^s_{mean} , (**e**) $P^w_{\max}/P^s_{\max}$, (**f**) P^w_{cent}/P^s_{cent} , (**g**) COF^w/COF^s , (**h**) $t^w_{\max}/t^s_{\max}$. '**1**' indicates the results of fixed N_w = 19 ($\Omega_x \approx 39.8$), and '**2**' indicates the results of fixed A = 3.7.

 doi:10.20944/preprints202404.1568.v1

Figure 5a.1 shows that the asperity contact ratio generally increases as the amplitude increases for most cases. The increase trends are similar for the wave directions of 0°, -30°, and -60°. That is, when the amplitude is relatively small, the asperity contact ratio is zero, meaning no asperity contact. However, for the longitudinal (−90°) waviness, there are significant asperity contacts even with the minimal amplitude used in the current simulations. Such differences between longitudinal and other directions of waviness also appeared in our previous Part I paper.

Figure 5a.2 shows that all the wave directions have similar trends of asperity contact ratio as the frequency increases. The asperity contact ratio first increases from zero to a maximum value and then decreases as the frequency increases. This phenomenon means that specific waviness frequencies may weaken the micro-EHL effects most in the mixed lubrication regime, resulting in the maximum asperity contact ratio. Moreover, considering the transformation of transverse (0°) waviness to longitudinal waviness (−90°), Figures 5a.1 and 5a.2 clearly show that the asperity ratios generally increase along with such a process.

All the $h^w_{\min}/h^s_{\min}$ ratios in Figures 5b.1 and 5b.2 are smaller than one, indicating the minimum film thickness decrease due to waviness. Moreover, as the amplitude or frequency increases, the EHL system works in the partial film regime; thus, the minimum film thickness is gradually reduced to zero, indicating that asperity contacts are occurring. When the wave direction turns from transverse (0°) to longitudinal (−90°), the amplitude or frequency value corresponding to the zero minimum film thickness decreases. This result shows again that the transverse waviness can enhance the EHL effects the most, while the longitudinal waviness has little positive effect on the EHL effects. This point is consistent with the results reported in our previous Part I paper [1].

Figures 5c.1 and 5c.2 show the h^w_{cent}/h^s_{cent} ratios. It is evident that the longitudinal waviness (θ = −90°) results in a different trend of the central film thickness ratios compared to the other three wave directions (θ = 0°, −30°, and −60°). In Figure 5c.1, when θ = 0°, −30°, and −60°, the central film thickness ratios are greater than one and decrease as the amplitude increases. When θ = −90°, the central film thickness is zero and does not change as the amplitude changes. In Figure 5c.2, when θ = 0°, −30°, and −60°, the central film thickness ratios are almost greater than one and follow an increasing trend as the frequency increases. When θ = −90°, a decreasing trend is observed as the frequency increases. Moreover, as the wave directions turn from θ = 0° to θ = −30°, the h^w_{cent}/h^s_{cent} ratios decrease. Thus, converting the transverse waviness to longitudinal waviness generally decreases the h^w_{cent}/h^s_{cent} ratio.

Figures 5d.1 and 5d.2 show the mean film thickness ratios. They have similar patterns to the central film thickness ratios shown in Figures 5c.1 and 5c.2. In Figure 5d.1, when θ = 0°, −30°, and −60°, the mean film thickness ratios are greater than one, while θ = −90°, the mean film thickness ratios are smaller than one. Moreover, when θ = 0°, −30°, the mean film thickness ratios increase as the amplitude increases. In comparison, the mean film thickness ratios decrease as the amplitude increases when θ = -60°, −90°. In Figure 5d.2, when the frequency is not greater than 19, the four directions of waviness correspond to mean film thickness ratios greater than one. The h^w_{mean}/h^s_{mean} ratios increase as the frequency increases. When the frequency is greater than 19, the mean film thickness ratios still increase as the frequency increases for θ = 0°, −30°. While for θ = -60°, −90°, the mean film thickness decreases rapidly as the frequency increases to around 34. Then, the mean film thickness ratio increases again for θ = −60° and decreases slowly for θ = −90°. Furthermore, the mean film thickness ratio can be smaller than one when θ = −90°. These results mean that the h^w_{mean}/h^s_{mean} ratios decrease as the wave directions turn from transverse to longitudinal. Moreover, the effects of amplitude and frequency on the mean film thickness ratios show different trends as the wave directions turn to longitudinal.

Considering Figures 5a to 5d comprehensively, it can be concluded that converting transverse waviness to longitudinal waviness decreases the EHL effects in terms of the film thickness under most circumstances. This point is the same as that drawn from the simulations within the full film regime. This should be because converting the waviness from transverse to longitudinal decreases the waviness's equivalent frequency in the direction of the relative motion (X-direction). The

 doi:10.20944/preprints202404.1568.v1

deviation in the surface geometry in the direction of the relative motion plays a critical role in generating hydrodynamic effects. According to the discussion in Section 3.1, the frequency decrease in the *X*-direction usually decreases the EHL effects regarding the film thickness.

Furthermore, comparing the results regarding the film thickness in this paper (corresponding to partial film regime) with those in our previous Part I paper [1] (corresponding to full film regime), it can be found that the longitudinal waviness has more significant effects when the EHL system works in the partial film regime.

Figures 5e.1 and 5e.2 show that the $P_{\max}^{w}/P_{\max}^{s}$ ratios are significantly affected by the alterations in the wave directions. This phenomenon differs from that shown in the Part I paper, where the maximum pressure ratios are almost unaffected by wave directions except $\theta = -90°$. The maximum pressure ratios increase as the amplitude increases for most cases, as shown in Figure 5e.1. As the wave direction turns from transverse (0°) to longitudinal (−90°), the growth rate of such an increasing trend first increases and then decreases. The fastest case in the current simulations is the waviness, whose direction is −60°.

Figure 5e.2 shows similar trends, but the growth rate is also sensitive to the frequency of waviness. When the frequency is no greater than 13, the maximum pressure ratios increase as the frequency increases. Moreover, the corresponding growth rate is almost the same. When the frequency further increases to around 47, the maximum pressure ratios increase at a different rate corresponding to wave directions. The wave direction of −60° is still the fastest-increasing case. A sharp peak appears for the longitudinal waviness. As the frequency increases to the maximum value used in the current simulations, the increase rate corresponding to the transverse waviness gradually exceeds other wave directions. Overall, combining Figures 5e.1 and 5e.2, the longitudinal waviness produces the slightest increase in the maximum pressure.

Figure 5f.1 shows that the $P_{cent}^{w}/P_{cent}^{s}$ ratios vary differently as the amplitude increases when the wave direction changes. The central pressure ratio values can be greater or less than one. When θ = 0°, −60°, the variation range of the central pressure ratios is relatively small compared with that corresponding to θ = −30°, −90°. The minimum central pressure ratio is around 0.4 when the wave direction is −30° and the amplitude reaches 4.7. The maximum central pressure ratio is close to 1.3 when the wave direction is −30° and the amplitude is 5. In Figure 5f.2, the $P_{cent}^{w}/P_{cent}^{s}$ ratios are close to one and have slight differences when θ = 0°, −30°, and −60°. When θ = −90°, the central pressure ratio sharply peaks as the frequency increases. The maximum value is greater than 4 when the frequency is around 19. These results suggest that longitudinal waviness increases the central pressure, while the other wave directions have relatively small impacts on the central pressure.

Figures 5g.1 and 5g.2 provide the COF^{w}/COF^{s} ratios. It should be highlighted that the patterns are pretty much the same as those shown in Figures 5a.1 and 5a.2, representing the asperity contact ratios. This phenomenon is because the simulated EHL system works in the partial regime. When asperity contacts occur, the friction force between asperities is much greater than the viscous friction. The summation of asperity friction force and viscous friction equals the total friction force. Thus, the COF ratios show the same patterns as the asperity contact ratios. Another point to address is that the COF ratios can be smaller than one, meaning a friction reduction by incorporating waviness when the amplitude and frequency of waviness are appropriately designed (e.g., A=3.7, $\Omega_x \approx 67$, θ = 0° in Figure 5g.2). It should be noted that the longitudinal waviness cannot decrease the COF in most cases.

Figure 5h.1 shows that the $t_{\max}^{w}/t_{\max}^{s}$ ratios fluctuate as the amplitude increases. When θ = 0° or −30°, the maximum temperature rise ratio first slowly increases, rapidly decreases, and then increases again as the amplitude increases. When θ = −60° or −90°, the maximum temperature rise ratio slowly increases as the amplitude increases. These results suggest that the variation of the maximum temperature rise ratio corresponding to amplitude is sensitive to the wave directions. In Figure 5h.2, the results are pretty different from those in Figure 5h.1. The maximum temperature rise ratio for all four wave directions does not vary much when the frequency value is no greater than 34. As the frequency further increases, the maximum temperature rise ratio corresponding to the wave direction

 doi:10.20944/preprints202404.1568.v1

of 0° first increases rapidly, then the −30° and −60° waviness. The −90° waviness does not significantly increase the maximum temperature rise ratio. These results indicate that longitudinal waviness can reduce the maximum temperature rise within the EHL zone compared with other forms of directional waviness.

According to the discussions above, the waviness with θ = 0°, −30°, and −60° results in more similar patterns than those with longitudinal waviness (θ = −90°). In summary, waviness moving toward the longitudinal direction increases the asperity contact ratio, reduces the film thickness, and increases the COF. In the meantime, the maximum pressure increases, and the maximum temperature rise decreases as the wave direction turns from 0° to −60°. The central pressure is relatively slightly affected by changing the wave directions. The increase in COF is due to the rise of asperity contact ratios, which dominate in generating friction force. In our previous Part I paper, the COF reduces when the transverse waviness turns to longitudinal waviness because the system works in a full film regime.

The longitudinal (θ = −90°) waviness is expected to result in different patterns than other wave directions. In our previous Part I paper, such phenomena have been thoroughly analyzed. The reason is that the longitudinal waviness does not change the initial surface geometry in the relative motion direction. This means little additional EHL effect is generated as the longitudinal waviness passes the Hertzian contact zone. Therefore, the current paper does not discuss the results separately with longitudinal waviness. However, all the contour maps can be found in Supplemental Material S1 for readers' convenience.

3.3. The Influences of the Load and Speed

According to Section 3.2, the transverse waviness (θ = 0°) generates the most significant additional EHL effects in most cases. Thus, the results regarding transverse waviness are discussed to represent and highlight the influences of the load and speed.

The two cross lines of each contour map, i.e., the lines with A = 3.7 or $\Omega_x \approx 39.8$ (N_w = 19), were also extracted. Then, the extracted lines with the fixed wave direction (θ = 0°), the same type of performance parameter, and the same constant A or Ω_x were plotted in one graph. In each graph, the four curves representing the four combinations of loads (w = 200 N or 500 N) and speeds (u_s = 0.3 m/s or 2 m/s) show the impacts of the load and speed. The four combinations are indexed as i: (w = 500 N, u_s = 0.3 m/s), ii: (w = 200 N, u_s = 0.3 m/s), iii: (w = 500 N, u_s = 2 m/s), and iv: (w = 200 N, u_s = 2 m/s). As the working conditions change from i to iv, the corresponding smooth central (or minimum) film thickness increases (see Table 2). The thinner the film thickness is, the harsher the working conditions are. For one wave direction, there are sixteen such graphs. They are organized as sub-figures. Figure 6 shows the graphs for transverse waviness, where indices a to h represent the seven performance parameters, where '1' and '2' indicate the results of the fixed $\Omega_x \approx 39.8$ (N_w = 19) and A = 3.7, respectively.

 doi:10.20944/preprints202404.1568.v1

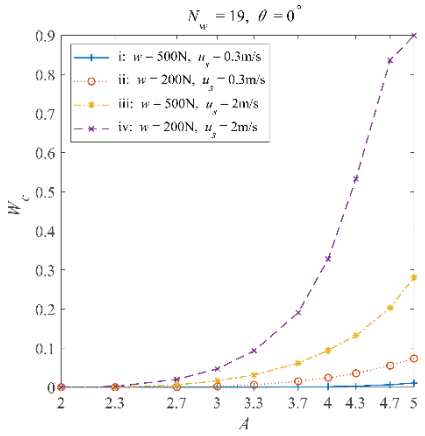

(a.1)

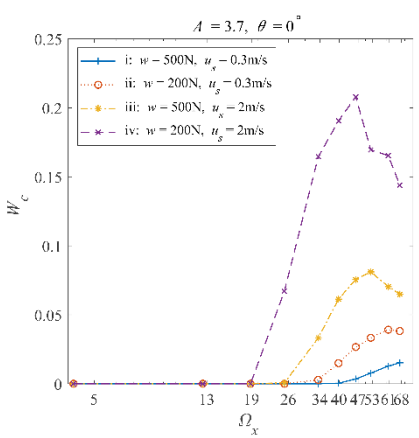

(a.2)

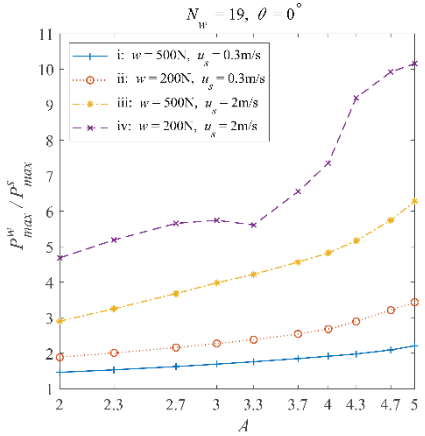

(e.1)

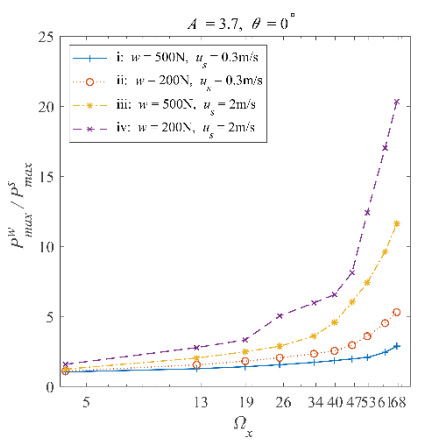

(e.2)

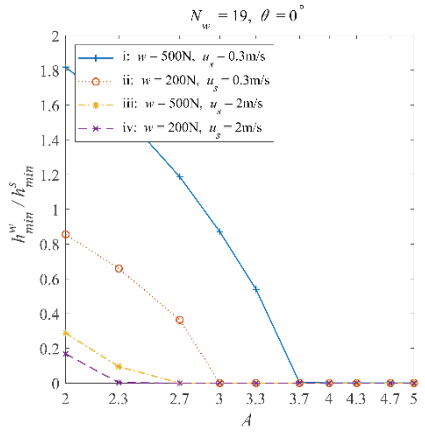

(b.1)

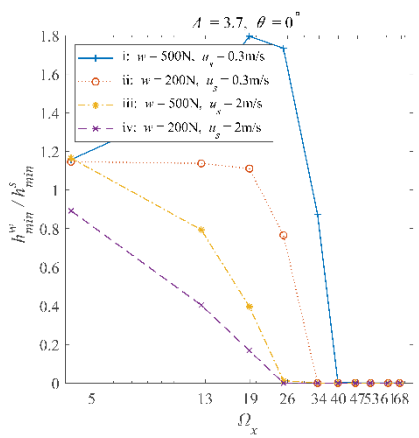

(b.2)

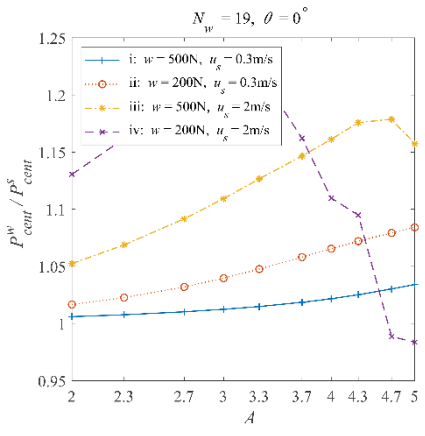

(f.1)

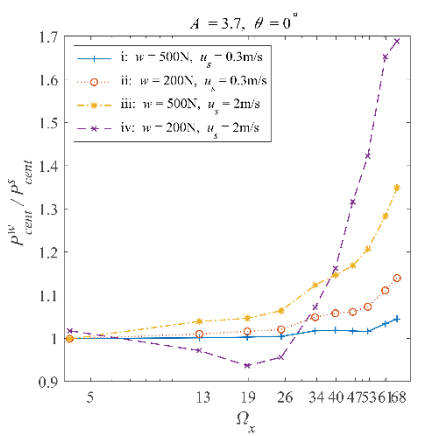

(f.2)

 doi:10.20944/preprints202404.1568.v1

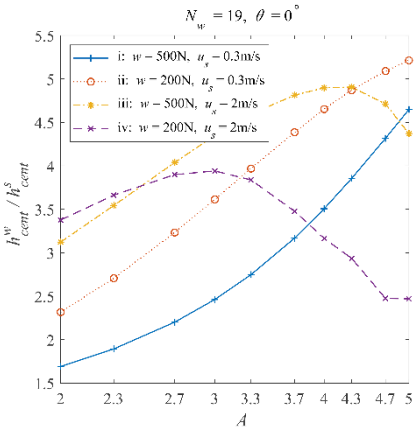

(**c.1**)

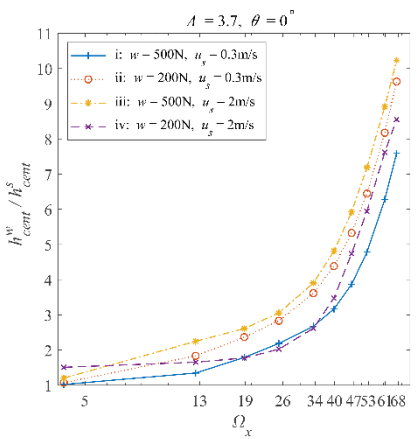

(**c.2**)

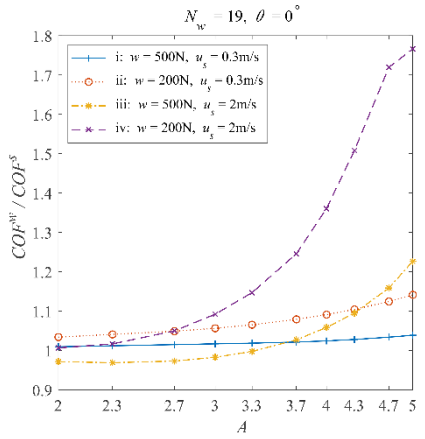

(**g.1**)

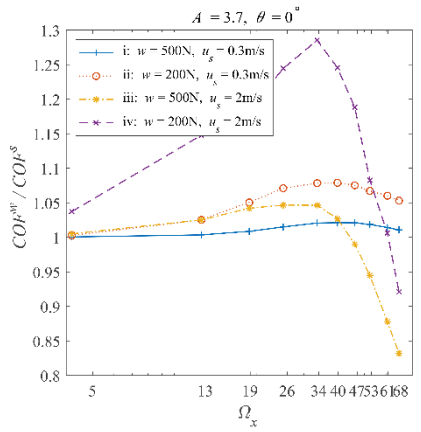

(**g.2**)

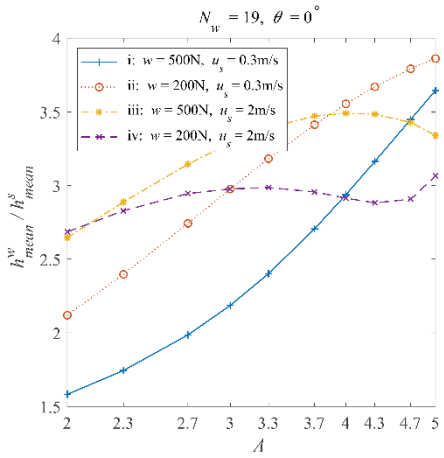

(**d.1**)

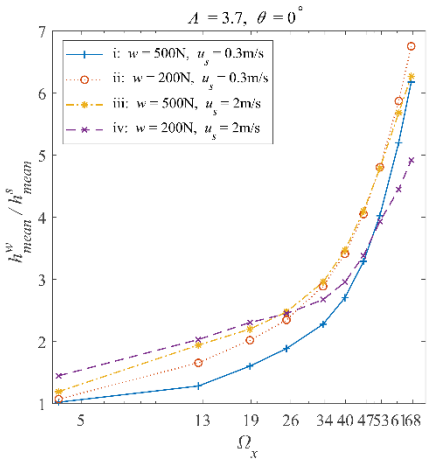

(**d.2**)

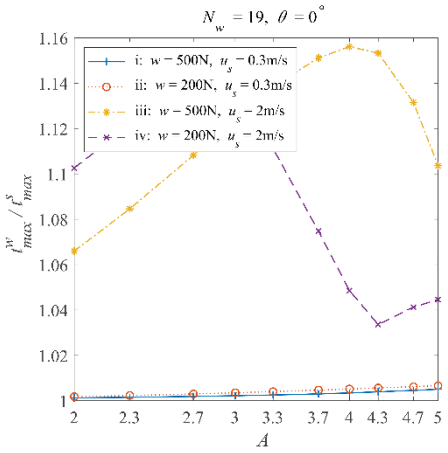

(**h.1**)

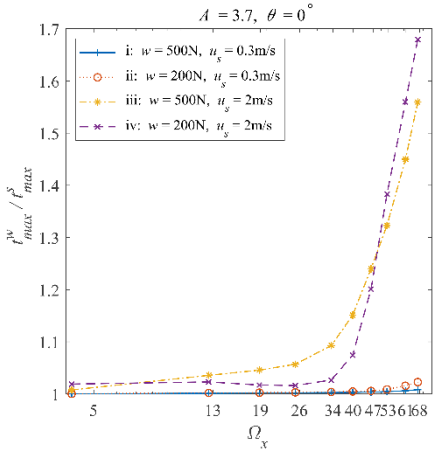

(**h.2**)

Figure 6. Performance parameters with θ = 0°, w = 200 N, 500 N, u_s = 0.3 m/s, 2 m/s. Indices a to h are (**a**) W_c, (**b**) $h^w_{\min}/h^s_{\min}$, (**c**) h^w_{cent}/h^s_{cent}, (**d**) h^w_{mean}/h^s_{mean}, (**e**) $P^w_{\max}/P^s_{\max}$, (**f**) P^w_{cent}/P^s_{cent}, (**g**) COF^w/COF^s, (**h**) $t^w_{\max}/t^s_{\max}$. '**1**' indicates the results of fixed N_w = 19 ($\Omega_x \approx 39.8$), and '**2**' indicates the results of fixed A = 0.09.

 doi:10.20944/preprints202404.1568.v1

Figures 6a.1 and 6a.2 show that different working conditions significantly affect the asperity contact ratio. The W_c increases as the working condition changes from i to iv for most of the amplitude and frequency values. Such results indicate that mild working conditions result in relatively severe asperity contacts. In order to understand this phenomenon, the definition of the amplitude and frequency should be considered. Equations 3 to 5 show that the non-dimensional amplitude and frequency are related to the central film thickness and Hertzian contact radius corresponding to the smooth EHL. Thus, although the non-dimensional amplitude and frequency shown in Figures 6a.1 and 6a.2 are the same for the four working conditions, the dimensional amplitude and frequency are very different.

For example, in mild working conditions, such as working condition iv, the film thickness is thicker than other harsher working conditions, showing more significant EHL effects. However, according to equations 3, the same non-dimensional amplitude A results in a much greater dimensional amplitude for working condition iv than for other harsher working conditions. Such a difference in the dimensional wavy amplitude can neutralize the significant EHL effects of mild working conditions and result in relatively severe asperity contacts compared to harsh working conditions.

Figures 6b.1 and 6b.2 show that the minimal film thickness ratio, $h^w_{\min}/h^s_{\min}$, is significantly affected by different working conditions. The minimal film thickness ratio decreases from greater to smaller than one as the working condition turns from i to iv for most of the A and Ω_x values. This phenomenon indicates that waviness can increase the minimum film thickness under harsh working conditions. When the working conditions become mild (i to iv), the waviness gradually decreases the minimum film thickness. Figures 6c and 6d show that as the working condition turns from harsh (i) to mild (iv), the central film thickness ratio, h^w_{cent}/h^s_{cent}, and mean film thickness ratio, h^w_{mean}/h^s_{mean}, show an increasing trend.

Figures 6e and 6f illustrate the influences of the working conditions on the maximum pressure ratio, $P^w_{\max}/P^s_{\max}$, and the central pressure ratio, P^w_{cent}/P^s_{cent}. It shows that changing the working conditions from harsh (i) to mild (iv) increases the maximum and central pressure ratios in most cases. It should be noted again that incorporating waviness increases the maximum pressure no matter which working condition is used. As for the central pressure, decreasing it using specific waviness is possible.

Figures 6g.1 and 6g.2 show that the effects of waviness on the COF are the most significant at the mildest condition in the current simulations (condition iv: w = 200 N, u_s = 2 m/s). Another point is that the COF can be reduced by incorporating waviness with specific amplitudes and frequencies, regardless of the working conditions used. On the other hand, adjusting the amplitudes and waviness can increase the COF. One should carefully choose the amplitude and frequency of waviness based on their purposes.

Figures 6h.1 and 6h.2 indicate that the maximum temperature rise is more closely related to the speed value. For a higher speed (u_s = 2 m/s, working conditions iii and iv), the maximum temperature rise ratio changes more significantly as the amplitude or frequency changes. This phenomenon is expected, as the shear heat causes the temperature to rise nearly proportionally to the relative speed.

In summary, the effects of the working conditions on the EHL performance with waviness are generally enhanced as the working conditions become mild. Such trends are the same as those in the previous Part I paper, considering only the full film lubrication regime. Moreover, the non-dimensional amplitude and frequency values are determined by the characteristic parameters of an EHL problem (Equations (3) –(5)). Thus, the same non-dimensional waviness indicates that the waviness incorporated is the same regarding scales compared with the EHL system. Based on the simulated results shown above, it is clear that the same non-dimensional waviness leads to very different results for different working conditions. These results indicate the nonlinear nature of the EHL system. A case-by-case basis should be followed to analyze the effects of waviness on the EHL performance.

 doi:10.20944/preprints202404.1568.v1

Furthermore, two points should be addressed. First, the minimum film thickness could be increased by incorporating waviness when the working conditions are harsh. Second, the COF and maximum temperature rise results are more sensitive to changes in speed. This should be because the friction force and the temperature rise are closely related to the shear stresses, which are strongly affected by the relative speed.

3.4. Further Remarks on the Contour Maps

The eight performance parameters are not independent as they characterize the same EHL system. According to the results discussed above, generally, incorporating waviness that enforces the system works in the partial film regime increases the asperity contact ratio and decreases the minimum film thickness. The central and mean film thickness values are increased at the same time. In most cases simulated in the current work, the maximum pressure, COF, and maximum temperature rise values increase. It should be highlighted that the minimum film thickness and COF can be reduced simultaneously with specific combinations of waviness parameters (amplitude A, frequency Ω_x, and direction θ) even in the partial film lubrication regime. However, the maximum pressure and maximum temperature rise values, at the same time, still increase.

Another point that needs to be noted is that incorporating waviness benefits the EHL system when it has harsh working conditions. Therefore, if one wishes to utilize waviness as a beneficial factor in an EHL system working in the partial film regime, one should balance its influences on the different performance parameters. The simulated data and corresponding contour maps can be references for this purpose. The other important point is combining the current simulation results with those in our previous Paper I to make a series of contour maps covering a more comprehensive lubrication regime and amplitude range.

4. Conclusions

This paper is a continuity work of the previous Part I paper (doi:10.3390/lubricants10120368). It studies the responses of a typical point-contact elastohydrodynamic lubrication (EHL) problem to multiscale roughness that is mimicked by artificially generated waviness with different amplitudes, frequencies, and directions. More specifically, it focuses on the partial film lubrication regime. A series of working conditions were considered in simulations as well. Eight performance parameters of an EHL system were extracted from the simulation results. The ratios of these parameters with and without waviness were discussed in detail. The main conclusions are as follows:

1. The transverse and oblique waviness lead to similar results. When the amplitude increases to initiate asperity contacts, waviness with a high frequency and large amplitude can generate severe asperity contact ratio, a thicker lubricant film in terms of the mean and central film thickness, with a higher maximum pressure, and result in a greater COF, with a higher temperature rise. The minimum film thickness decreases in most cases but still can increase with specific combinations of waviness parameters.
2. The waviness moving toward the longitudinal direction increases the asperity contact ratio, reduces the film thickness, and increases the COF. In the meantime, the maximum pressure increases, and the maximum temperature rise decreases as the wave direction turns from 0° to −60°. The central pressure is relatively slightly affected by changing the wave directions. The increase in COF is due to the rise of asperity contact ratios, which dominate in generating friction force.
3. The effects of the working conditions on the EHL performance with waviness are generally enhanced as the working conditions become mild. The minimum film thickness can be increased, and the COF can be decreased when the working condition is harsh, even in the partial film lubrication regime. The COF and maximum temperature rise values are more sensitive to the change in the speed than the change in the load.
4. One who wishes to utilize waviness as a beneficial factor in an EHL system working in the partial film lubrication regime should balance its influences on the different performance parameters. The simulated data and corresponding contour maps can be referenced (see Supplementary Material S1).

 doi:10.20944/preprints202404.1568.v1

Furthermore, combining this paper and the previous Part I paper, one can make a series of contour maps covering a more comprehensive lubrication regime and amplitude range, which could be a helpful reference for researchers to understand the effects of waviness on point EHL systems comprehensively.

Supplementary Materials: The following supporting information can be downloaded at the website of this paper posted on Preprints.org. 'Supple-mental Material S1.zip, including the files: 'Contour plots.docx' , 'ReadMe.pdf', and 'Results_all_X_partial.mat'.

Author Contributions: Conceptualization, Yuechang Wang and Ying Liu; Funding acquisition, Yuechang Wang and Ying Liu; Methodology, Yuechang Wang and Ying Liu; Project administration, Yuechang Wang and Ying Liu; Software, Yuechang Wang; Supervision, Ying Liu; Validation, Yuechang Wang; Writing – original draft, Yuechang Wang; Writing – review & editing, Yuechang Wang and Ying Liu. All authors have read and agreed to the published version of the manuscript.

Funding: This research was funded by the Shenzhen Science and Technology Innovation Commission, grant number GXWD20231129144211001, Shenzhen Talent Program, grant number, SZTP4202301629, and Harbin Institute of Technology, Shenzhen, grant number 20220068. National Natural Science Foundation of China (51975315).

Data Availability Statement: The data that support the findings of this study are available from the corresponding author, Y.W., upon reasonable request.

Acknowledgments: Supported by Center of High performance computing, Tsinghua University。.

Conflicts of Interest: The authors declare no conflict of interest. The funders had no role in the design of the study; in the collection, analyses, or interpretation of data; in the writing of the manuscript; or in the decision to publish the results.

Nomenclature

a	dimensional amplitude of the waviness, m
A	non-dimensional amplitude of waviness
b	radius of the Hertzian contact zone, m
M, N	number of grids in the X and Y directions, respectively
COF^w/COF^s	ratio of the COF with and without waviness
$h^w_{\min}/h^s_{\min}$	ratio of the minimum film thickness with and without waviness
h^w_{cent}/h^s_{cent}	ratio of the central film thickness with and without waviness
h^w_{mean}/h^s_{mean}	ratio of the mean film thickness with and without waviness
N_T	time step for the termination of the simulation
N_w	number of waves in the solution domain
$P^w_{\max}/P^s_{\max}$	ratio of the maximum pressure with and without waviness
P^w_{cent}/P^s_{cent}	ratio of the central pressure with and without waviness
r_θ	waviness in direction θ, m
$t^w_{\max}/t^s_{\max}$	ratio of the maximum temperature rise with and without waviness
$\overline{t}$	non-dimensional time in the simulation
$\Delta\overline{t}$	non-dimensional time interval of the simulation
u_1	velocity of the smooth surface, m/s
u_2	velocity of the waviness, m/s
u_s	sum of u_1 and u_2, m/s
U	non-dimensional speed
w	load, N
W_c	asperity contact ratio
X_s, X_e	non-dimensional start and end coordinates of the solution domain in the X direction
Y_s, Y_e	non-dimensional start and end coordinates of the solution domain in the Y direction

X_s', Y_s'	non-dimensional start of waviness at $\bar{t}=0$ with the wave direction θ
α	viscosity–pressure coefficient in the Barus viscosity law, Pa^{-1}
θ	wave direction, degree
Λ_x	non-dimensional wavelength of the waviness
Ω_x	non-dimensional frequency of the waviness

References

1. Wang, Y., et al., *Understanding the Influences of Multiscale Waviness on the Elastohydrodynamic Lubrication Performance, Part I: The Full-Film Condition.* Lubricants, 2022. **10**(12): p. 368.10.3390/lubricants10120368.
2. Vakis, A.I., et al., *Modeling and simulation in tribology across scales: An overview.* Tribology International, 2018. **125**: p. 169-199.10.1016/j.triboint.2018.02.005.
3. ARCHARD, J.F., *ELASTIC DEFORMATION AND THE LAWS OF FRICTION.* PROCEEDINGS OF THE ROYAL SOCIETY OF LONDON SERIES A-MATHEMATICAL AND PHYSICAL SCIENCES, 1957. **243**(1233): p. 190-205.
4. Sayles, R.S. and T.R. Thomas, *Surface topography as a nonstationary random process.* Nature, 1978. **271**(5644): p. 431-434.10.1038/271431a0.
5. Mandelbrot, B.B., *The fractal geometry of nature*. Vol. 173. 1983, New York: W. H. Freeman.
6. MAJUMDAR, A. and C.L. TIEN, *Fractal characterization and simulation of rough surfaces.* Wear, 1990. **136**(2): p. 313-327.
7. Majumdar, A. and B. Bhushan, *Fractal Model of Elastic-Plastic Contact Between Rough Surfaces.* Journal of Tribology, 1991. **113**(1): p. 1-11.10.1115/1.2920588.
8. Bhushan, B. and A. Majumdar, *Elastic-plastic contact model for bifractal surfaces.* Wear, 1992. **153**(1): p. 53-64.10.1016/0043-1648(92)90260-f.
9. Persson, B.N.J., *Theory of rubber friction and contact mechanics.* The Journal of Chemical Physics, 2001. **115**(8): p. 3840-3861.10.1063/1.1388626.
10. Müser, M.H., et al., *Meeting the Contact-Mechanics Challenge.* Tribology Letters, 2017. **65**(4): p. 118.10.1007/s11249-017-0900-2.
11. Persson, B.N.J., et al., *On the nature of surface roughness with application to contact mechanics, sealing, rubber friction and adhesion.* Journal of Physics: Condensed Matter, 2004. **17**(1): p. R1-R62.10.1088/0953-8984/17/1/r01.
12. Majumdar, A. and C.L. Tien, *Fractal network model for contact conductance.* Journal of Heat Transfer, 1991. **113**(3): p. 516-525.10.1115/1.2910594.
13. Barber, J.R., *Bounds on the electrical resistance between contacting elastic rough bodies.* Proceedings of the Royal Society of London. Series A: Mathematical, Physical and Engineering Sciences, 2003. **459**(2029): p. 53-66.doi:10.1098/rspa.2002.1038.
14. Longuet-Higgins, M.S. and G.E.R. Deacon, *Statistical properties of an isotropic random surface.* Philosophical Transactions of the Royal Society of London. Series A, Mathematical and Physical Sciences, 1957. **250**(975): p. 157-174.doi:10.1098/rsta.1957.0018.
15. Nayak, P.R., *Random process model of rough surfaces.* Journal of Lubrication Technology, 1971. **93**(3): p. 398-&.10.1115/1.3451608.
16. Patir, N. and H.S. Cheng, *Average flow model for determining effects of 3-dimensional roughness on partial hydrodynamic lubrication.* Journal of Lubrication Technology-Transactions of the ASME, 1978. **100**(1): p. 12-17.
17. Patir, N. and H.S. Cheng, *Application of average flow model to lubrication between rough sliding surfaces.* Journal of Lubrication Technology-Transactions of the ASME, 1979. **101**(2): p. 220-230.
18. Patir, N. and H.S. CHENG, *Effect of Surface Roughness Orientation on the Central Film Thickness in EHD Contacts %\ 2015-11-21 17:39:00*. 1979.
19. Zhu, D. and X.L. Ai, *Point contact EHL based on optically measured three-dimensional rough surfaces.* JOURNAL OF TRIBOLOGY-TRANSACTIONS OF THE ASME, 1997. **119**(3): p. 375-384.
20. Minet, C., N. Brunetiere, and B. Tournerie, *MIXED LUBRICATION MODELLING IN MECHANICAL FACE SEALS.* PROCEEDINGS OF THE STLE/ASME INTERNATIONAL JOINT TRIBOLOGY CONFERENCE 2008, 2009: p. 477-479.
21. Ren, N., et al., *A Three-Dimensional Deterministic Model for Rough Surface Line-Contact EHL Problems.* JOURNAL OF TRIBOLOGY-TRANSACTIONS OF THE ASME, 2009. **131**(0115011).

22. Demirci, I., et al., *Multiscale Analysis of the Roughness Effect on Lubricated Rough Contact.* Journal of Tribology, 2013. **136**(1): p. 011501-011501-8.10.1115/1.4025222.
23. Lorentz, B. and A. Albers, *A numerical model for mixed lubrication taking into account surface topography, tangential adhesion effects and plastic deformations.* Tribology International, 2013. **59**: p. 259-266.10.1016/j.triboint.2012.08.023.
24. Zhu, D. and Q.J. Wang, *Effect of Roughness Orientation on the Elastohydrodynamic Lubrication Film Thickness.* JOURNAL OF TRIBOLOGY-TRANSACTIONS OF THE ASME, 2013. **135**(0315013).
25. Zhu, D., J.X. Wang, and Q.J. Wang, *On the Stribeck Curves for Lubricated Counterformal Contacts of Rough Surfaces.* Journal of Tribology-Transactions of the Asme, 2015. **137**(2).10.1115/1.4028881.
26. Zhang, X., Y. Xu, and R.L. Jackson, *A mixed lubrication analysis of a thrust bearing with fractal rough surfaces.* Proceedings of the Institution of Mechanical Engineers, Part J: Journal of Engineering Tribology, 2019. **234**(4): p. 608-621.10.1177/1350650119867242.
27. Li, L. and J. Yang, *Surface roughness effects on point contact elastohydrodynamic lubrication in linear rolling guide with fractal surface topographies.* Industrial Lubrication and Tribology, 2018. **70**(4): p. 589-598.10.1108/ILT-04-2017-0092.
28. Pei, J., et al., *Mixed elastohydrodynamic lubrication analysis of line contact with Non-Gaussian surface roughness.* Tribology International, 2020. **151**: p. 106449.https://doi.org/10.1016/j.triboint.2020.106449.
29. Venner, C.H. and A.A. Lubrecht, *An Engineering Tool for the Quantitative Prediction of General Roughness Deformation in EHL Contacts Based on Harmonic Waviness Attenuation.* Proceedings of the Institution of Mechanical Engineers, Part J: Journal of Engineering Tribology, 2005. **219**(5): p. 303-312.10.1243/135065005x33973.
30. Bair, S. and W.O. Winer, *The high pressure high shear stress rheology of liquid lubricants.* Journal of Tribology, 1992. **114**(1): p. 1-9.10.1115/1.2920862.
31. Pu, W., J. Wang, and D. Zhu, *Progressive Mesh Densification Method for Numerical Solution of Mixed Elastohydrodynamic Lubrication.* Journal of Tribology, 2015. **138**(2): p. 021502-021502.
32. Wang, W.Z., et al., *Solution agreement between dry contacts and lubrication system at ultra-low speed.* Proceedings of the Institution of Mechanical Engineers, Part J: Journal of Engineering Tribology, 2010. **224**(10): p. 1049-1060.10.1243/13506501jet774.
33. Venner, C.H. and A.A. Lubrecht, *Numerical Analysis of the Influence of Waviness on the Film Thickness of a Circular EHL Contact.* Journal of TribologyJournal of Tribology, 1996. **118**(1): p. 153.
34. He, T., et al., *Experimental and Numerical Investigations of the Stribeck Curves for Lubricated Counterformal Contacts.* Journal of Tribology, 2016. **139**(2).10.1115/1.4034051.
35. Reddyhoff, T., A. Schmidt, and H. Spikes, *Thermal Conductivity and Flash Temperature.* Tribology Letters, 2019. **67**(1): p. 22.10.1007/s11249-018-1133-8.
36. Liu, H.C., et al., *Influences of solid and lubricant thermal conductivity on traction in an EHL circular contact.* Tribology International, 2020. **146**: p. 106059.https://doi.org/10.1016/j.triboint.2019.106059.
37. Habchi, W. and S. Bair, *The role of the thermal conductivity of steel in quantitative elastohydrodynamic friction.* Tribology International, 2020. **142**: p. 105970.https://doi.org/10.1016/j.triboint.2019.105970.